ON ANISOTROPY EFFECTS IN DUCTILE FRACTURE: THEORY AND APPLICATIONS

A. A. Benzerga[1], J. Besson[1] and A. Pineau[1]
[1] Ecole des Mines de Paris, Centre des Matériaux,
UMR CNRS 7633, BP 87, F91003 Evry Cedex

ABSTRACT

This paper proposes a general framework for post-coalescence modelling. Constitutive relations include an ad-hoc yield surface depending on the first and second invariants of the stress tensor along with evolution laws for the microstructural variables, namely ligament size, void shape and void spacing ratio. The loss of stress carrying capacity is then a natural outcome of the formulation. Anisotropic failure in a pipe steel is modelled using a finite element implementation of the model.

KEYWORDS

Anisotropic sheets, porous plastic solids, plastic anisotropy, void shape, post–coalescence

INTRODUCTION

Micromechanical modelling of coalescence is key to understanding the role of microstructure on the fracture properties of ductile solids. In a previous work [1], microstructural effects on the onset of coalescence were investigated; instead of being fitted on experiments, critical porosities were predicted and used to simulate failure in notched bars. Incorporating void shape effects is crucial at low stress triaxiality even with no initial anisotropy [2, 3]. At high stress triaxiality, the influence of void shape is less an issue, but the material undergoes as much deformation after the onset of coalescence as prior to it [4]. This raises the issue of modelling post–coalescence. To do so, void shape effects have to be accounted for [1]. In this paper, a new approach is used, which is based on a recent micromechanical model for post–coalescence [5]. A series of finite element calculations are carried out and compared with experiments conducted on a C–Mn pipe steel containing elongated inclusions.

MODELLING

Pre–coalescence Behaviour

The constitutive framework is that of anisotropic porous plastic solids. Anisotropy here refers to the plastic anisotropy of the matrix material [6] and to void shape effects [2]. For a solid containing spheroidal cavities and respecting transverse isotropy, the plastic potential reads in a frame $(\underline{\mathbf{e}}_x, \underline{\mathbf{e}}_y, \underline{\mathbf{e}}_z)$ related to cavities

$$\Phi = C\frac{||\underset{\sim}{\Sigma}' + \eta\Sigma_h\underset{\sim}{\mathbf{X}}||^2}{\sigma_\star^2} + 2q_w(g+1)(g+f)\cosh\left(\frac{\kappa\Sigma_h}{\sigma_\star}\right) - (g+1)^2 - {q_w}^2(g+f)^2 = 0 \tag{1}$$

where $(\,)'$ denotes deviatoric quantities, $\sigma_\star$ is the matrix flow strength, f is the void volume fraction and

$$\Sigma_h = \alpha_2(\Sigma_{xx} + \Sigma_{yy}) + (1 - 2\alpha_2)\Sigma_{zz} \tag{2}$$

$$\underset{\sim}{\mathbf{X}} = \frac{1}{3}(-\underline{\mathbf{e}}_x \otimes \underline{\mathbf{e}}_x - \underline{\mathbf{e}}_y \otimes \underline{\mathbf{e}}_y + 2\,\underline{\mathbf{e}}_z \otimes \underline{\mathbf{e}}_z) \tag{3}$$

$$q_w = 1 + (q-1)\cosh^{-1} S \tag{4}$$

where $\underline{\mathbf{e}}_z$ is the common axis of the voids and g, κ, α_2, η and C are scalar functions of the porosity, f, and the shape parameter, S, defined as the logarithm of the void aspect ratio. Analytical expressions of these functions can be found in [2, 5]. The evolution of porosity is the consequence of mass conservation and is derived from the potential Φ assuming normal flow [7]. The evolution of S is given by (see [2])

$$\dot{S} = \frac{3}{2}\left[1 + \frac{9}{2}h_{\mathcal{T}}(\mathcal{T})(1-\sqrt{f})^2\frac{\alpha_1 - \alpha_1^G}{1-3\alpha_1}\right]D'_{zz} + 3\left(\frac{1-3\alpha_1}{f} + 3\alpha_2 - 1\right)D_m \tag{5}$$

$$h_{\mathcal{T}} = 1 - \frac{\mathcal{T}^2 + \mathcal{T}^4}{9} \tag{6}$$

where D_m^{p} and D'^{p}_{zz} are the mean part of the plastic strain rate, $\underset{\sim}{\mathbf{D}}^{\mathrm{p}}$, and the axial component of $\underset{\sim}{\mathbf{D}}'^{\mathrm{p}}$ respectively. α_1 and ${\alpha_1}^G$ depend on S only and $\mathcal{T}$ is the stress triaxiality ratio.

Plastic anisotropy is introduced through the first term which appears in the development of the norm $||\ ||$ in (1). Based on an equivalent extension in the case of spherical or cylindrical cavities [6], it is suggested to replace the Mises stress by the Hill quadratic stress [8] using a frame $(\underline{\mathbf{E}}_X, \underline{\mathbf{E}}_Y, \underline{\mathbf{E}}_Z)$ pointing onto the principal directions. Correlatively, $\sigma_\star$ is replaced by the flow strength along X. Principal axes of orthotropy are taken to be the void axes and only loadings parallel to these axes are considered such that cavities do not rotate relative to the frame of orthotropy, Fig. 1. In this case, it is reasonable to assume that the voids rotate at the same velocity as the material. The voids, however, are allowed to be perpendicular to the loading; see Figure 1(b). In this case initial axisymmetry is broken and an approximated spheroidal shape is still assumed in average [5]. The first finite–element simulations using this constitutive model were discussed by Benzerga *et al.* [9].

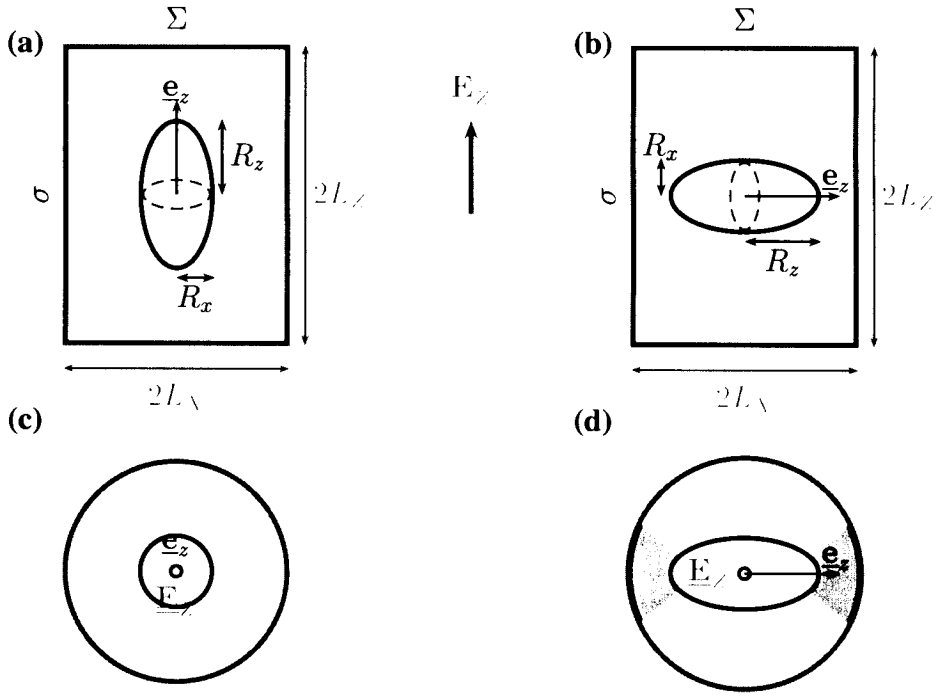

Figure 1: Schematic view for the treatment of initial anisotropy. *(a) case of* $\underline{\mathbf{e}}_z \parallel \underline{\mathbf{E}}_Z$ *with* $\chi \equiv R_x/L_X$ *given by (9), (b) case of* $\underline{\mathbf{e}}_z \perp \underline{\mathbf{E}}_Z$ *with* $\chi \equiv R_z/L_X$ *if* $S > 0$ *and* $\chi \equiv R_x/L_X$ *if* $S < 0$. *(c) and (d) views in the plane of coalescence corresponding to (a) and (b) respectively.*

Onset of Coalescence

Coalescence is taken to occur when the smallest ligament between neighbouring voids attains its limit–load [10]. A three–dimensional criterion for void coalescence is written as

$$(1-\chi^2)\,C_f(\chi, S) = \left(\frac{2}{3} + \mathcal{T}\right)\frac{3\,\underset{\sim}{\Sigma}' : \underset{\sim}{\mathbf{H}} : \underset{\sim}{\Sigma}'}{2\,\sigma_\star^2} \tag{7}$$

where χ is the ligament size defined as the ratio of current void diameter along X to current spacing along X, L_X; see Figure 1. $\underset{\approx}{\mathbf{H}}$ is Hill's tensor previously defined and C_f is the limit–load factor given by

$$C_f = 0.1\left(\frac{\chi^{-1}-1}{e^{-S}+\alpha\chi^{-1}}\right)^2 + 1.2\sqrt{\chi^{-1}} \tag{8}$$

where modification from an original form [11] has been included following [5]. In [11] C_f diverges for penny–shaped cracks. Here $\alpha = 0.14$. The expression of χ depends on the loading configuration [5]

$$\chi^3 = \begin{cases} \dfrac{3}{2} f\lambda\, \mathrm{e}^{-S} & S < 0 \\ \dfrac{3}{2} f\lambda & S > 0 \quad \text{and} \quad \underline{\mathbf{e}}_z \perp \underline{\mathbf{E}}_Z \end{cases} \tag{9}$$

where $\lambda \equiv L_Z/L_X$ is the spacing ratio. Refer to [1] for an evaluation of criterion (7) in the case $\underline{\mathbf{e}}_z \parallel \underline{\mathbf{E}}_Z$

Post–coalescence Behaviour

The model used here is based on [5] and defined by a set of constitutive relations including an expression of the yield surface along with appropriate evolution laws for the shape parameter and the ligament size ratio, χ.

Yield function

When criterion (7) is fulfilled, the behaviour is no longer given by (1–5). Indeed, localization, which pertains to post–coalescence, unambiguously sets the normal to the yield surface. The latter is then defined by

$$\Phi^{(c+)}(\underset{\approx}{\Sigma}, \chi, S) = \frac{\Sigma_{\mathrm{eq}}}{\sigma_\star} + \frac{1}{2}\frac{\underset{\approx}{\mathbf{I}} : \underset{\approx}{\Sigma}}{\sigma_\star} - \frac{3}{2}(1-\chi^2)\, C_f(\chi, S) \tag{10}$$

(10) is rigorously stated for isotropic plasticity. Using Σ_{eq} according to Hill, as previously defined, is the simplest heuristic extension to plastic anisotropy.

Evolution laws

These are appropriately formulated in terms of the shape parameter, S, and the ligament size ratio, χ. For an arbitrary convex shape, the ligament size ratio is given by (provided that $\underline{\mathbf{e}}_z \parallel \underline{\mathbf{E}}_Z$)

$$\chi = \left[3\gamma f \lambda \mathrm{e}^{-S}\right]^{1/3} \tag{11}$$

γ is a shape factor: $\gamma = 1/2$ for a spheroid and $\gamma = 1$ for a cone. The rates of χ and S are given by (see [5])

$$\dot{\chi} = \frac{3\gamma}{2}\frac{\lambda}{W}\left[\frac{3}{2\chi^2} - 1\right] D_{\mathrm{eq}} \tag{12}$$

$$\dot{S} = \frac{9}{4}\frac{\lambda e^{-S}}{\chi}\left[\frac{2(1+\gamma)}{3} - \frac{\gamma}{\chi^2}\right] D_{\mathrm{eq}} \tag{13}$$

The full model is implemented in the finite element code ZeBuLoN [12].

MATERIAL IDEALIZATION

The material modelled is a pipe steel cut from a rolled sheet of grade X52. The frame related to the sheet is (L,T,S) with L being the rolling axis, T the transverse axis and S the through–thickness axis. Material characterisation and tensile tests on round notched bars are presented elsewhere [1]. Due to the working process, the material exhibits a marked anisotropy of plastic flow, which can be represented using a quadratic yield criterion with the following Hill coefficients: $h_{\mathrm{L}} = 0.96$, $h_{\mathrm{T}} = 0.88$, $h_{\mathrm{S}} = 1.28$, $h_{\mathrm{TS}} = 1.30$, $h_{\mathrm{SL}} = 1.15$ and $h_{\mathrm{LT}} = 1.09$. The main inclusions involved in the damage process are equiaxed particles (mainly oxides),

with a volume fraction of 0.00035, and manganese sulfides (MnS stringers) with a volume fraction of 0.0004 [5]. Inclusion shape and spacing were characterised using metallography and Dirichlet tessellation techniques. For MnS particles, the average representative element is made of a stringer parallel to L and 1.5μm thick, embedded in a box with the dimensions: $\overline{S}_{\rm S} \approx 353\,\mu$m, $\overline{S}_{\rm L} \approx 420\,\mu$m and $\overline{S}_{\rm T} \approx 223\,\mu$m. The equiaxed particles were found to be isotropically distributed [5]. The hardening law used in the computations is

$$\sigma_\star(p) = R_0 + a\,p + Q\,\left(1 - e^{-b\,p}\right) \tag{14}$$

where p is the cumulated plastic strain, $R_0 = 426$MPa, $a = 239.8$MPa, $Q = 162.3$MPa and $b = 16.1$.

Nucleation is supposed to be homogeneous and the material is assigned an initial porosity, f_0, which is equal to the volume fraction of both sulfides and oxides or to that of sulfides only, depending on the fracture mechanism. To handle the 3D shape of sulfides, one needs to define an equivalent spheroidal shape based on the formula: $W_0 \equiv \sqrt{\overline{W}^{\rm T}\,\overline{W}^{\rm S}}$, where $\overline{W}^{\rm T} = 32$ and $\overline{W}^{\rm S} = 7.5$ are respectively the length–to–thickness and length–to–width ratios of the particle. The average initial shape parameter is then $S_0 = \ln(W_0) = 2.74$. Similarly, the average spacing ratio is calculated as $\lambda_0^{\rm L} \equiv \sqrt{\overline{\lambda}^{\rm T}\,\overline{\lambda}^{\rm S}}$, for loadings parallel to L, with $\overline{\lambda}^{\rm T} = 1.20$ and $\overline{\lambda}^{\rm S} = 1.90$ which gives $\lambda_0^{\rm L} = 1.5$. Using $\overline{\lambda}^{\rm L} = 0.63$ one also gets $\lambda_0^{\rm T} = 0.6$ for loadings parallel to T.

RESULTS

Notched bars are denoted AN_ζ where ζ is ten times the ratio of notch radius to the minimal section diameter. Results are shown for two of the tested geometries: AN_{10} and AN_2. 3D meshes are used for 1/8 of the specimen. For computational efficiency, the elements close to the minimal section are initially flat in order to have them roughly square at incipient fracture. The element size in the plane of coalescence is 325μm. Boundary conditions are imposed in terms of a prescribed displacement on the top of the specimen. Other symmetry conditions are used to eliminate any rigid–body motion as in [1]. Quadratic quadrilateral sub–integrated elements with updated Lagrangian formulation are used. In line with experimental observations, the values of the shape factor γ are 0.8 and 0.5 for L–loading and T–loading respectively.

Figure 2 shows selected curves of force versus diameter reduction, normalised by the initial diameter, $\Phi_0 = 1.95$mm. Experimental results are represented by points. These have been inferred from interrupted tests in order to follow the development of plastic anisotropy. For a major stress oriented along L (i.e. L–loading), the initial microstructure was $f_0 = 0.075\%$, $S_0 = 1.95$ and $\lambda_0^{\rm L} = 1.5$. It is assumed that the two populations of particles, MnS and oxides, nucleate voids. Comparison of Figs 2(a) and (b) clearly shows that the previous assumption is quite good for the AN_2 specimen but that ductility of the AN_{10} specimen is overestimated. It is likely that the onset of coalescence at low triaxiality be due to voids nucleated at equiaxed particles, as supported by experimental observations [5].

For T–loading, we relax the assumption upon the initial equivalent microstructure. Hence, for the AN_{10} specimen, only MnS particles were taken into account and the values $f_0 = 0.04\%$, $S_0 = 2.35$ and $\lambda_0^{\rm T} = 0.6$ were used. On the other hand, the values $f_0 = 0.075\%$, $S_0 = 2.35$ and $\lambda_0^{\rm T} = 1$ were used in the case of the AN_2 specimen, which means that the equiaxed particles are incorporated as for their contribution to the volume fraction and the distribution of initial voids. Comparison of Figs 2(c) and (d) suggests that the latter assumption provides better correspondence with experiments.

These results show that it is possible to predict the fracture anisotropy in the modelled steel provided that one has knowledge about the initial microstructure and fracture mechanisms. It is worth noting that two types of damage anisotropy emerge in these calculations. The first one is related to the shape and distribution of the MnS particles. At a given constraint, i.e. at fixed ζ, the material is much more resistant when the major stress is oriented along the longitudinal direction and the model accounts for this initial anisotropy. Second, there is an induced anisotropy due to plastic orthotropy of the matrix material as discussed in [6]. Contours of constant void volume fraction in any specimen loaded along L show that the development of damage is much more rapid in the transverse direction, although diameter reduction is lower.

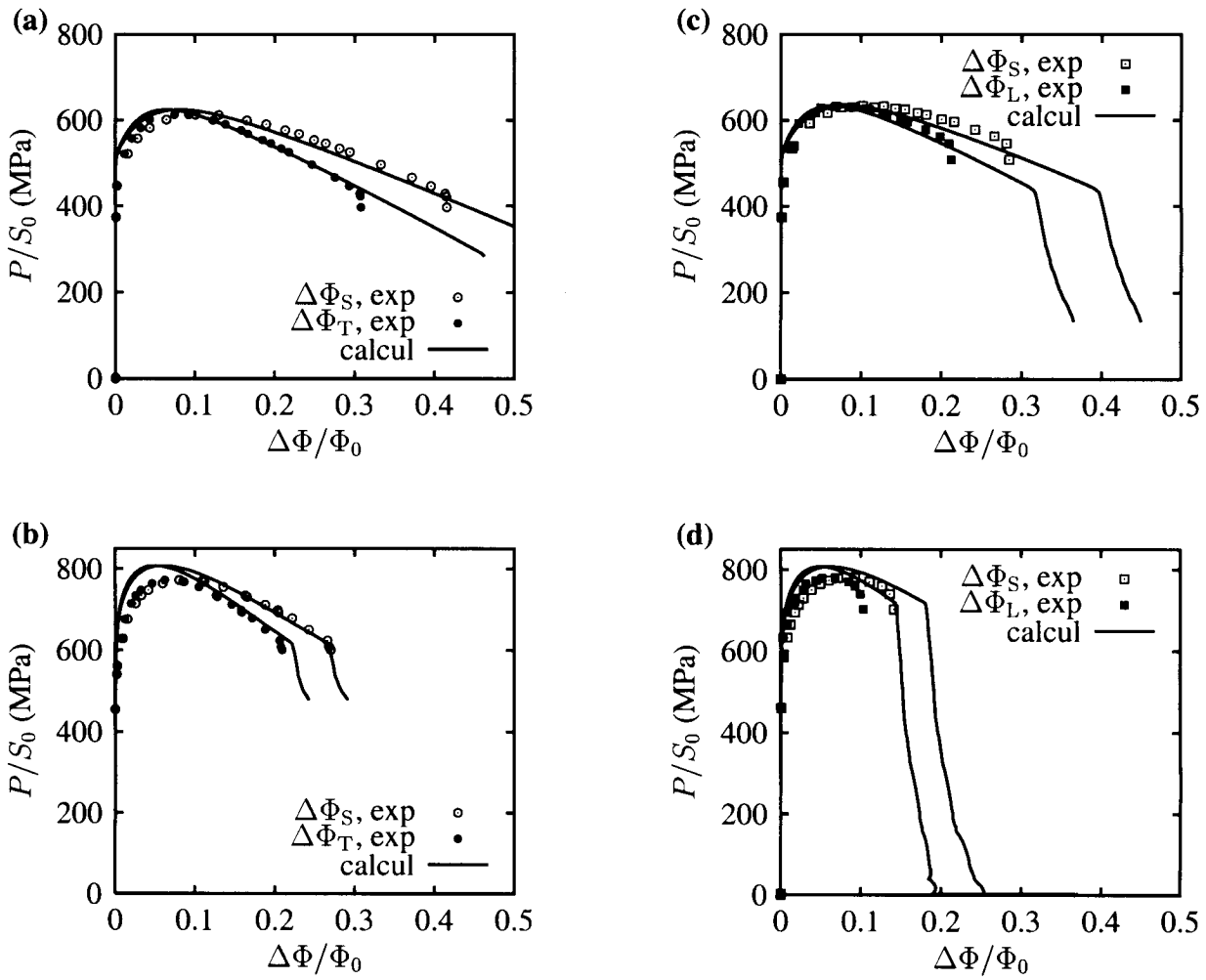

Figure 2: Load *vs* diameter reduction curves for round notched bars. *(a) L–loading and* $\zeta = 10$*; (b) T–loading and* $\zeta = 10$*; (c) L–loading and* $\zeta = 2$*; (d) T–loading and* $\zeta = 2$*. Points are for experimental results.*

Anisotropy of the fracture process is illustrated in Figure 3 in the case of the $AN_{10}T$ specimen. When criterion (7) is attained at the center of the specimen, Fig. 3(a), the macroscopic force drops for the first time (see Fig 2(c)) although there is no macroscopic crack yet. This is indicated by the activation of the post–coalescence index `pc` in Fig. 3(a) while the fracture index `broken` is still deactivated. The fact that `pc` $\neq 0$ means that the ligament size has attained its limit load. As a consequence, the behaviour of corresponding elements is given by (10-13). Upon continued deformation, the region which undergoes post–coalescence enlarges anisotropically as a result of plastic anisotropy. At stage (b), a macroscopic crack initiates. Crack propagation then occurs along the elements which have undergone post–coalescence until the force is reduced to zero. It is worth emphasizing that the material loses all stress carrying capacity as a natural outcome of ligament reduction as described by the post–coalescence model.

CONCLUSIONS

Microstructure effects were investigated in an anisotropic sheet using a micromechanical model which accounts for post–coalescence. No adjustable factor was used. Microstructural parameters needed as an input of the simulations were inferred from quantitative metallography. Hence, the calculations are by no means biased towards the experimental results. This in turn allowed for a full discussion of pertinent mechanisms that cause fracture. In a $AN_{10}L$ specimen, the average triaxiality is 0.8 and the elongated cavities nucleated on MnS particles hardly lead to coalescence; coalescence is rather due to equiaxed particles. This is the reason why ductility was overestimated in this case. In the sharply notched specimen AN_2L, however, the triaxiality is

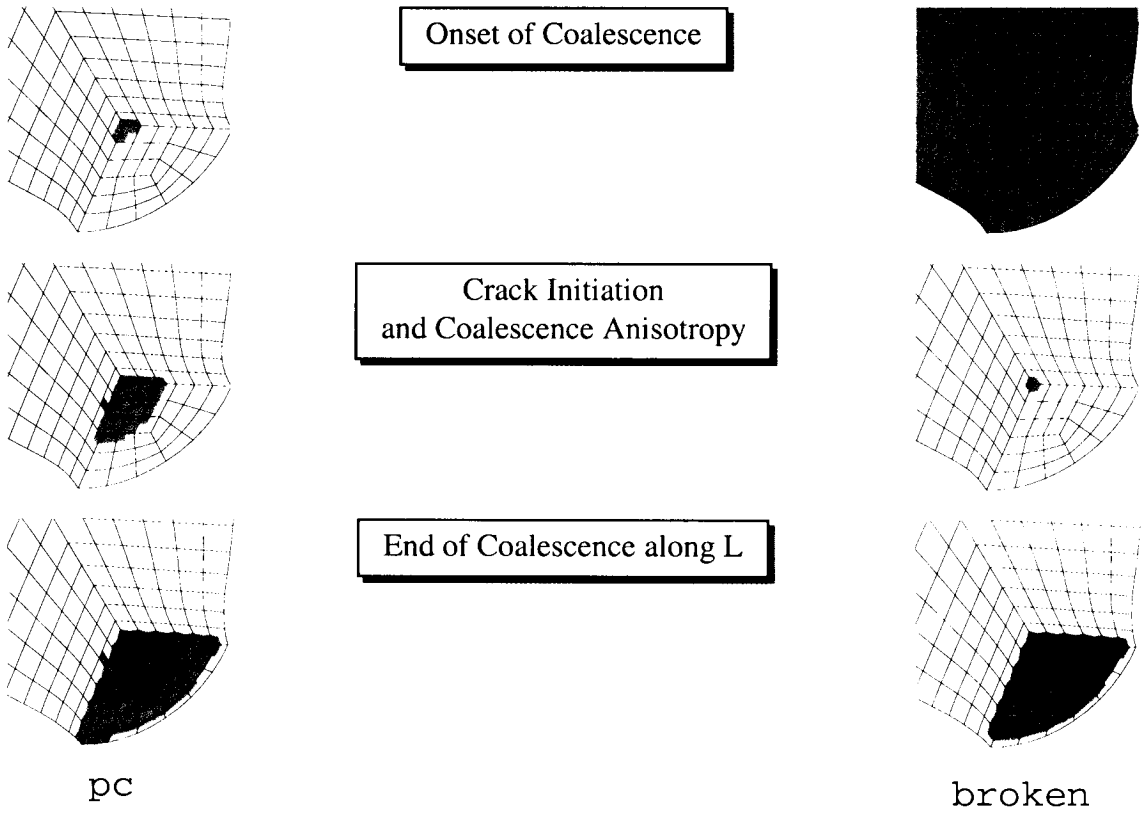

Figure 3: Coalescence anisotropy and crack growth in the notch region of AN_{10} specimen loaded along T–direction. *(a) post–coalescence index* `pc`*; elements undergoing coalescence are painted black. (b) Broken elements (i.e.* $\chi \equiv 1$*) are painted black.*

high enough to activate both populations of cavities and the results are then more consistent with experimental ones. Similar conclusions can be drawn for T–loading provided that the equiaxed particles are incorporated in the spatial arrangement.

Acknowledgements
Support from Gaz de France (Direction de la Recherche) is gratefully acknowledged. AAB thanks F. Curie for helpful contribution to the quantitative metallography.

References

[1] A. A. Benzerga, J. Besson, and A. Pineau. *J. Eng. Mat. Tech.*, 121(2):221–229, 1999.
[2] M. Gologanu, J.-B. Leblond, G. Perrin, and J. Devaux. In P. Suquet, editor, *Continuum Micromechanics*, pp 61–130. Springer–Verlag, 1995.
[3] P. Ponte Castañeda and M. Zaidman. *J. Mech. Phys. Solids*, 42:1459–1495, 1994.
[4] J. Koplik and A. Needleman. *Int. J. Solids Structures*, 24(8):835–853, 1988.
[5] A. A. Benzerga. PhD thesis, Ecole des Mines de Paris, March 2000. parts in english.
[6] A. A. Benzerga and J. Besson. *Eur. J. Mech.*, 2001. accepted.
[7] A. L. Gurson. *J. Eng. Mat. Tech.*, 99:2–15, 1977.
[8] R. Hill. *Proc. Roy. Soc. London A*, 193:281–297, 1948.
[9] A. A. Benzerga, J. Besson, R. Batisse, and A. Pineau. In M. W. Brown, E. R. de los Rios, and K. J. Miller, editors, 12^{th} *Eur. Conf. on Fracture*, pp 715–720. ESIS, Eur. Group on Fracture Publication, 1998.
[10] A. H. Cottrell. In B. L. Averbach, editor, *Fracture*, pp 20–53. Chapman and Hall, London, 1959.
[11] P. F. Thomason. *Acta Metallurgica*, 33(6):1079–1085, 1985.
[12] J. Besson and R. Foerch. *Comput. Methods Appl. Mech. Engrg*, 142:165–187, 1997.